

# Efficient time dependent Wannier functions for ultrafast dynamics

Cristian M. Le<sup>1,\*</sup>, Hannes Hübener<sup>1,†</sup>, Ofer Neufeld<sup>2,1,‡</sup> and Angel Rubio<sup>1,3,§</sup>

<sup>1</sup>*Max Planck Institute for the Structure and Dynamics of Matter and  
Center for Free Electron Laser Science, 22761 Hamburg, Germany*

<sup>2</sup>*Schulich Faculty of Chemistry, Technion - Israel Institute of Technology, Haifa, Israel*

<sup>3</sup>*Center for Computational Quantum Physics (CCQ),  
The Flatiron Institute, 162 Fifth Avenue, New York NY 10010.*

Time-dependent Wannier functions were initially proposed as a means for calculating the polarization current in crystals driven by external fields. In this work, we present a simple gauge where Wannier states are defined based on the maximally localized functions at the initial time, and are propagated using the time-dependent Bloch states obtained from established first-principles calculations, avoiding the costly Wannierization at each time step. We show that this basis efficiently describes the time-dependent polarization of the laser driven system through the analysis of the motion of Wannier centers. We use this technique to analyze highly nonlinear and non-perturbative responses such as high harmonic generation in solids, using the hexagonal boron nitride as an illustrative example, and we show how it provides an intuitive picture for the physical mechanisms.

## I. INTRODUCTION

Wannier functions[1, 2] form a single-particle orthonormal basis in solid-state crystals that are widely used as an alternative to Bloch orbitals. Especially, maximally localized Wannier functions (MLWFs) have proven to be of great practical use, because they give chemical intuition to first-principles numerical results of static and thermodynamic properties[2]. In this representation one can visualize properties typically studied in molecular systems, such as hybridization, covalency and ionicity, in solid-state crystals[3–5], and provide the basis for the implementation of the modern theory of polarization[6–8]. Wannier functions also play an important role in the formulation and evaluation of response properties, because of their close relation to polarization[9], Born effective charges[10], Berry phase and curvature[11] etc., making them particularly useful in describing various topology related properties. The Wannier functions have been expanded to perturbation theory[12], Floquet theory[13], and time propagation[14, 15] in order to obtain localized basis representations in each of these domains. They have also been used as interpolators to extract electron-phonon coupling[16–19].

MLWFs are widely used as a convenient and well-defined orbital basis to derive tight-binding models of materials from first principles. These models are especially useful in analyzing complex materials such as highly correlated systems[20], because they allow the reduction of the correlated problem to a set of few active atomic orbitals per site, for instance through methods like constrained RPA[21]. To describe dynamical properties in such systems one normally propagates these lattice

models built on top of a static MLWFs basis set. This requires in principle the wannierization of all unoccupied states into which the system evolves, relying on prior intuition of the dynamic processes involved and often entailing increased computational cost.

Another proposed approach is to make the Wannier functions themselves time-dependent and calculate the observables directly in this basis[14]. Despite the early recognition of this application, Wannier function propagation has not been systematically pursued as a practical and efficient computational strategy and the precise definition has not yet been explored. The one notable case is an approach where the wannierization is done with the constraint to maximally localize the states at each time-step of the out-of-equilibrium driven system[15, 22]. This approach showed good agreements between the electronic polarization and experimental absorption spectra[15], and it retained the intuitive chemical representation in that process. However, besides the high computational cost associated with maximally localizing the Wannier functions at each time-step, there is also a conceptual issue in that this basis set can have discontinuities in time as the global minima of the MLWFs changes, leading to discontinuous derived observables[15].

The most direct application of time-dependent Wannier functions is to study the dynamics of the dielectric polarizations and its current, particularly beyond the regime of response theory, for instance high-order-harmonic generation (HHG) in solids which is not accessible via perturbation theory[23–25]. With the advances in ultrafast lasers, HHG in solid-state materials have been studied both experimentally and computationally. One common calculation method is using tight-binding models[26–34], but in order to fully capture the dynamics, particularly the interband dynamics, these models need to be expanded to include the unoccupied bands[35], increasing the computational cost. MLWFs have been shown to be especially useful for analyzing HHG, but the basis set here is static corresponding to the ground state system[36–41], unlike other useful basis sets which

\* cristian.le@mpsd.mpg.de

† hannes.huebener@mpsd.mpg.de

‡ ofer.neufeld@gmail.com

§ angel.rubio@mpsd.mpg.de

evolve with the Hamiltonian, like Houston[25, 42–45] or Floquet-Bloch states[46–52]. On the other hand, first-principles methods, like the real-time time-dependent density functional theory (TD-DFT)[53], incorporate all of these dynamics within the occupied orbitals only[54–60]. Here we show that the time evolution of the Wannier functions are able to incorporate all of these dynamics within a far smaller basis by combining these methods.

Here we propose and numerically study a definition of the time-dependent Wannier functions, where the wannierization step is done only once on the ground state (i.e at  $t = 0$ ), and the time-dependent Wannier states are determined by the time-dependent Bloch states, which we take from established first-principles calculations. We use this definition to study HHG in both non-interacting model system and ab-initio in hexagonal boron nitride (h-BN). We show that with this definition, the current can be described purely from the motion of Wannier centers in a wide range of laser driving profiles, providing an intuitive analogue for the dipole acceleration in finite systems but applied to periodic solids.

## II. TIME DEPENDENT WANNIER FUNCTION DEFINITIONS

Here, we consider time-dependent Wannier functions of the following form

$$\Phi_{n\mathbf{R}}(\mathbf{r}, t) = \sum_i \int_{BZ} U_{i\mathbf{k}}^{n\mathbf{R}} f_{i\mathbf{k}}(t) \Psi_{i\mathbf{k}}(\mathbf{r}, t) d^3\mathbf{k}, \quad (1)$$

where  $\Phi$  are the time-dependent Wannier functions,  $\Psi$  are the time-dependent Bloch states,  $U$  is the Wannier transformation matrix, which is calculated only once at the ground state to give the MLWF, and  $f$  is a time-dependent phase compensation function that we introduce in order to retain the localized nature of the Wannier functions. Note, that one could also re-compute  $U$  over time, but this would not be numerically efficient or guarantee a continuous evolution of the time-dependent Wannier states. Instead, we here express the time-dependence of the Wannier functions via the phase factor  $f$  and time-dependent Bloch states  $\Psi$  only, which does not result in maximally localized functions, but it does guarantee continuous evolution while still maintaining a high degree of localization. We explore three such phase compensation functions

$$f_{i\mathbf{k}}^{\text{none}}(t) = 1 \quad \forall i, \mathbf{k}, t, \quad (2)$$

$$f_{i\mathbf{k}}^{\text{static}}(t) = e^{i\epsilon_{i\mathbf{k}}^0 t}, \quad (3)$$

$$f_{i\mathbf{k}}^{\text{int}}(t) = e^{i \int_0^t \epsilon_{i\mathbf{k}}(\tau) d\tau}, \quad (4)$$

where we either do not perform any phase compensation (Eq. (2)), compensate for the static band energy  $\epsilon^0$  (Eq. (3)), or compensate for the instantaneous energy expectation value (Eq. (4))

$$\epsilon_{i\mathbf{k}}(t) = \langle \Psi_{i\mathbf{k}}(t) | \hat{H}(t) | \Psi_{i\mathbf{k}}(t) \rangle. \quad (5)$$

The reasoning behind these choices is to explore the scope and importance of such phase compensation. The  $f^{\text{static}}$  is the trivial initial state, or field free, evolution, while  $f^{\text{int}}$  takes the driving field into account, via the expectation value of the time-dependent Hamiltonian  $\langle \hat{H}(t) \rangle$ , as well as changes in the character of the Bloch states during time-evolution. To analyze the differences of these definitions, we look at the evolution of the Wannier spread  $\Omega(t)$ :

$$\Omega_n(t) = \int_V \mathbf{r}^2 |\Phi_{n\mathbf{R}}(\mathbf{r}, t)|^2 d^3\mathbf{r} - |\mathbf{r}_{n\mathbf{R}}(t)|^2, \quad (6)$$

$$\mathbf{r}_{n\mathbf{R}}(t) = \int_V \mathbf{r} |\Phi_{n\mathbf{R}}(\mathbf{r}, t)|^2 d^3\mathbf{r}, \quad (7)$$

where we denote here  $\mathbf{r}_{n\mathbf{R}}(t)$  to be the time-dependent Wannier center.

We investigate the different time-dependent Wannier functions first by considering a non-interacting 1D electron system under a Mathieu potential with or without an external laser interaction  $\mathbf{A}(t)$

$$\hat{H}(t) = \frac{1}{2m} (\hat{\mathbf{p}} - e\mathbf{A}(t))^2 + \hat{V}, \quad (8)$$

$$V(x) = -V_0(1 + \cos(2\pi x/a)). \quad (9)$$

Here we choose some well studied parameters for the Mathieu potential  $V_0 = 0.37(E_h)$ ,  $a_0 = 8(a_0)$ , resulting in the static band structure shown in Fig. 1a. In this model we take the first two bands to be fully occupied, and for this section we focus on the dynamics of these valence band and the evolution of their corresponding Wannier function.

We first consider the stationary ground-state case

$$\mathbf{A}(t) = 0 \quad \forall t, \quad (10)$$

and let both the system and Eq. (1) evolve coherently in time. By definition, all observables are time-independent and in the ground state, as the system evolves with only a pure global phase which cancels out when evaluating observables. But the Wannier function basis from Eq. (1) is still time-dependent as it is obtained by summing up Bloch states that coherently interfere due to the different phase propagations of the band eigenvalues of the Bloch states (Fig. 1a). This effect is evident in Fig. 1b when evaluating the Wannier spread  $\Omega$  without external perturbation. Wannier functions  $f^{\text{none}}$  that do not do phase compensation (blue line) loose localisation very fast, with a timescale matching roughly the band energy bandwidth. This trivial dephasing effect is exactly compensated by the other two definitions (red and yellow lines) that show a spread that is independent of time. In Fig. 1b, the red and yellow lines are on top of each other because by definition they are equivalent ( $f^{\text{static}} \equiv f^{\text{int}}$ ) when there is no time-dependent perturbation. This behavior is the main motivation for the introduction of the phase compensation term  $f$  in our definition of the time-dependent Wannier functions (Eq. (1)).

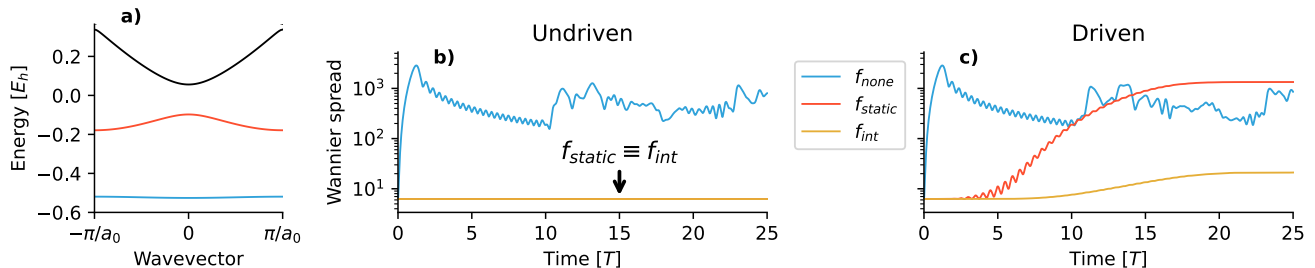


FIG. 1. Non-interacting 1D electron system under Mathieu potential. (a) Ground state bandstructure, (b) and (c) Wannier spread evolution without and with laser perturbation respectively. The band gap in (b) measures to  $\approx 0.154(E_h)$ .

Next, we consider the strongly driven non-perturbative case with a super-sine laser envelope[61]

$$A_x(t) = A_0 \sin\left(\frac{\pi t}{n_{\text{cyc}} T}\right)^{\frac{\pi}{\sigma}} \left| \frac{t}{n_{\text{cyc}} T} - \frac{1}{2} \right| \sin\left(\frac{2\pi t}{T}\right), \quad (11)$$

where we use the standard notations for the laser period  $T$ , and wavelength  $\lambda$

$$T = \frac{\lambda}{c}. \quad (12)$$

Here we look at the case with laser parameters: a peak laser intensity of  $I = 10^{11}(\text{W}/\text{cm}^2)$ , a wavelength of  $\lambda = 1500(\text{nm})$ , corresponding to  $\approx 0.198$  of the direct band gap, and a pulse duration of  $n_{\text{cyc}} = 25$  cycles. The Wannier spread evolution in this case are represented by Fig. 1c. The uncompensated evolution of the Wannier function ( $f^{\text{none}}$ , blue line) shows no significant difference from the undriven case, and we can disregard it as a practical definition of time-dependent Wannier functions. Looking at the  $f^{\text{static}}$  Wannier function (red line), we see that compensating for the static energy dephasing alone is also insufficient to retain the localized nature, as the spread evolves over time to become as fully delocalised as the uncompensated case. This is particularly evident when compared to the performance of  $f^{\text{int}}$  Wannier function (yellow line), which loses only some locality during this strong driving process. Note that the spread in Figs. 1b and 1c are shown on a logarithmic scale. We observe that even with the phase compensation of Eq. (4), the Wannier functions still retain some dynamics, and in the next section, we show that these dynamics can carry physical significance.

The model system here is simple enough that we can explore the evolution of the orbitals themselves in Fig. 2, where we plot the propagation of the Wannier function envelope for the case of the strong driving. Here we get a more intuitive view of how the  $f^{\text{int}}$  Wannier functions retain their localized nature. We can see that, although subtle, the Wannier function envelope is still evolving with the appearance of small oscillations in the tails of the envelope. This indicates that there is some non-trivial dynamics encoded in the Wannier-center and -spread. The time-dependent Wannier centers allow us to

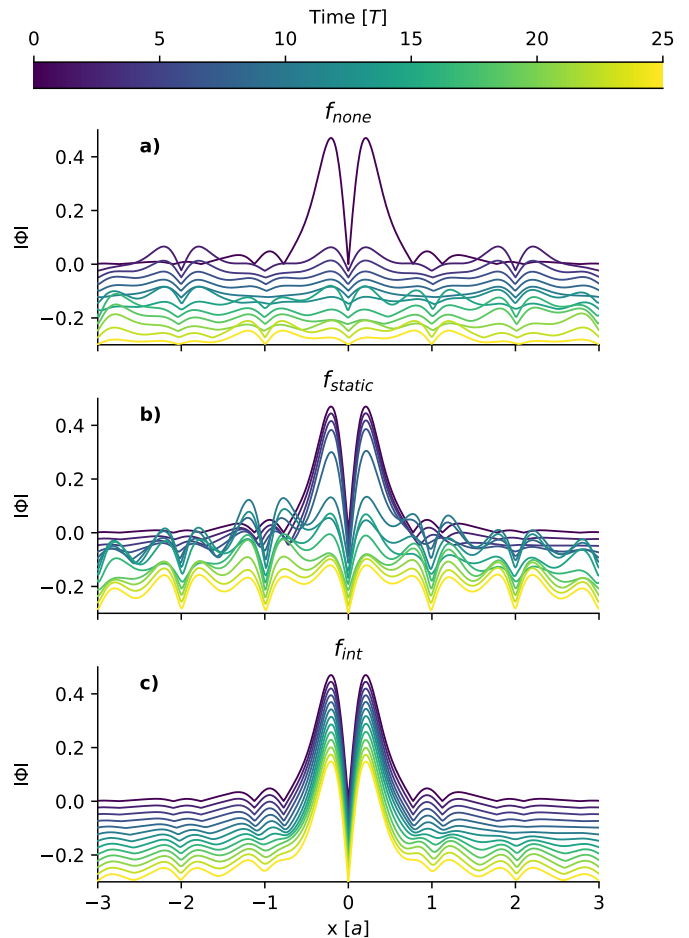


FIG. 2. Propagation of the Wannier function envelope in time. Each evaluated time-step is color coded according to the colorbar and shifted downwards.

generalize the theory of polarization to the time-domain, as discussed in the next section.

We note that this definition of time-dependent Wannier orbitals is closely related to other commonly used time-dependent single particle basis sets, such as the Peierls basis and the Houston basis, which we detail in

Appendix A. We especially note that the other basis do not change the shape of the single particle wave function envelope, and thus do not vary in their center and spread, as we have with the time-dependent Wannier functions given here. In Appendix A we also give a reasoning of why Eq. (4) is expected to work well for off-resonant excitation. Finally, we point out that here we do not discuss the generation of a time-dependent Wannier basis, but rather the construction of such states from a given time-evolution of Bloch states. This means that the time-dependence of the Bloch states is required to be available through an explicit time-propagation method and the Wannier functions discussed here can be thought of as a co-evolving complement basis that ideally spans the same space, but with far fewer states.

### III. HIGH-HARMONICS GENERATION WITH TIME-DEPENDENT WANNIER FUNCTIONS

In order to showcase the capability of the time-dependent Wannier functions as a basis set, we investigate the dynamic theory of polarization derived from the time-dependent Wannier centers[14]. We calculate the time-dependent Wannier function for a model non-interacting 1D system and a real-space TD-DFT calculation on h-BN. The calculations here were performed using *octopus*[62].

The main observable that we investigate is the polarization current derived from the electric dipole moment:

$$\mathbf{J}(t) = \frac{d\mathbf{P}(t)}{dt}, \quad (13)$$

where  $\mathbf{J}$  is the total electronic current and  $\mathbf{P}$  is the dynamic electronic polarization which we relate to the time-dependent Wannier functions[14] via

$$\mathbf{P}(t) = -\frac{e}{V} \sum_n \mathbf{r}_{n\mathbf{R}}(t). \quad (14)$$

We compare this current with the integrated current density calculated directly in the Bloch state representation[62] taken to be the reference current.

Here we analyze the HHG yield[54, 57–59, 63]

$$\xi(t) = \frac{d\mathbf{J}(t)}{dt}, \quad (15)$$

which we calculate either directly from the integrated current density evaluated in the full TD-DFT calculation by taking the time-dependent expectation value of the current operator, or from the polarization current that is in turn derived from the Wannier centers. We are primarily investigating the spectra of the HHG yield which we calculate from its Fourier transform

$$\xi(E) = \int e^{-iEt} \xi(t) dt. \quad (16)$$

We apply a Gaussian filter along the time-domain before evaluating its Fourier transform in order to clean up the residual oscillation at the tail of the laser pulse.

### A. Non-interacting 1D system

For the non-interacting 1D system we again take the Mathieu potential system that we explored in Section II, and we explore a wider range of laser parameters. The HHG in this system has been extensively studied using various calculation methods[35, 64]. In Fig. 3 we see a good agreement of the HHG yield derived from the Wannier functions (dashed red line) to the reference calculation using the Bloch states (solid blue line), across a wide range of laser parameters.

It is worth emphasizing how good the agreement of these results is. We reiterate that the time-dependent Wannier function definition is not unique, so there is no guaranteed correlation between the current obtained from the Wannier functions through Eqs. (13) and (14), and the observable current calculated from the Bloch states. This was clear from Section II, but it is even more evident if we compare the HHG spectra from Fig. 4, where it is clear that only the definition using Eqs. (1) and (4) gives us a polarization current that matches the reference observable. In principle, we would still be able to use the other Wannier functions as a time-dependent basis set, but in order to calculate an observable on such a basis, we would have to calculate the time-dependent occupation and/or expand the time-dependent Wannier basis set beyond the initially occupied ones in order to compensate for the difference in the Hilbert space. Here we show that time-dependent Wannier basis is an efficient basis set for capturing the local dynamics of the electrons in a more compact and localized representation. Importantly, this representation is able to capture the full range of non-linear processes in HHG, as can be seen in the agreement of the whole HHG spectra evaluated in Fig. 3.

One key usage of the Wannier functions is to gain chemical intuition of electronic structure and is worthwhile exploring how much of an intuitive picture of the dynamic processes is provided by our time-dependent Wannier functions. We now show that the time-dependent Wannier functions, indeed allow for an intuitive picture also for processes in the time domain and even in highly non-linear ones. First we Wannierize each band in Fig. 1a separately, i.e. without performing the sum over bands in Eq. (1), and we propagate these states individually according to Eqs. (1) and (4). We plot the contribution to the HHG spectra of each of these Wannier functions in Fig. 5, where we observe that effectively all of the HHG is contained in the dynamics of the top-valence Wannier function, even as the lower band Wannier function shows an equally strong linear response.

Next we perform the Wannierization procedure on both bands together, as done in all examples above, allowing the Wannier functions to mix and converge to a more localized basis set, and we propagate these states individually as before. This is more indicative to the general procedure that we might encounter when the bands are not as well separated that we could neatly converge

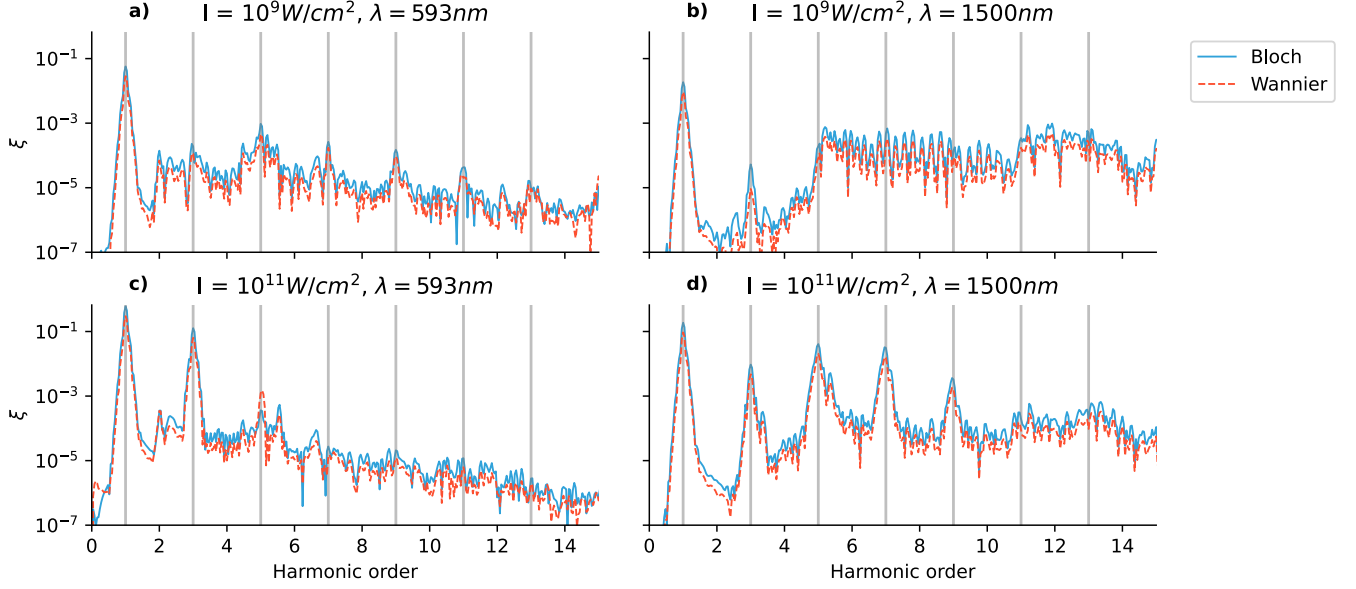


FIG. 3. HHG spectra of the non-interacting 1D system with varying laser interactions. The different lines correspond to the HHG yield calculated from the current calculated directly from the Bloch states or from the Wannier centers (Eq. (13)).

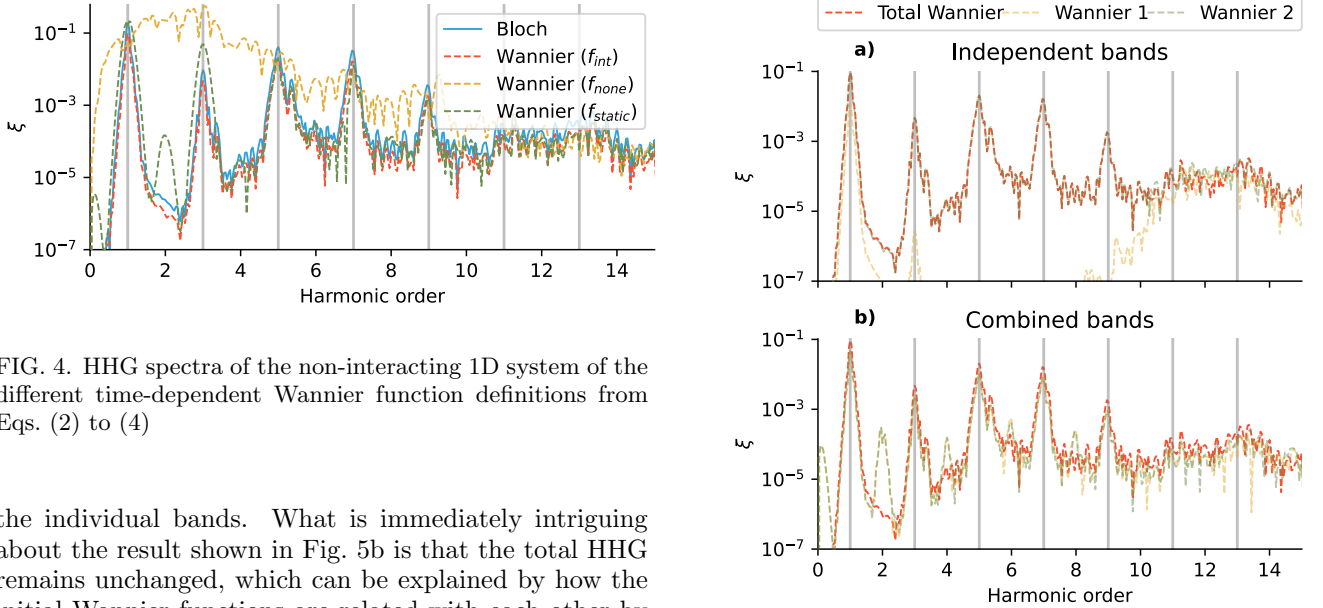


FIG. 4. HHG spectra of the non-interacting 1D system of the different time-dependent Wannier function definitions from Eqs. (2) to (4)

the individual bands. What is immediately intriguing about the result shown in Fig. 5b is that the total HHG remains unchanged, which can be explained by how the initial Wannier functions are related with each other by a unitary transformation. In this representation, the dynamics of the valence band is spread across both Wannier functions, and therefore we cannot visualize the HHG as nicely separated contributions as before. However, we can still observe an important effect: the individual Wannier states propagate with even order harmonics that cancel each other out due to the dynamical inversion symmetry in the model[65]. This shows that the individual trajectories of Wannier centers of mixed band character can break the symmetry, however the dynamics of the whole set of Wannier centers is restoring the symmetry. This can be thought of in analogy to the motion of individual atoms in phonons modes, that only collectively

form the eigenmode of the lattice.

## B. Hexagonal-BN

To show the generality of this approach we now consider a realistic system in 3D, h-BN which we drive with similarly strong laser profiles. Although the sys-

FIG. 5. HHG spectra of the non-interacting 1D system with different initial Wannier functions.

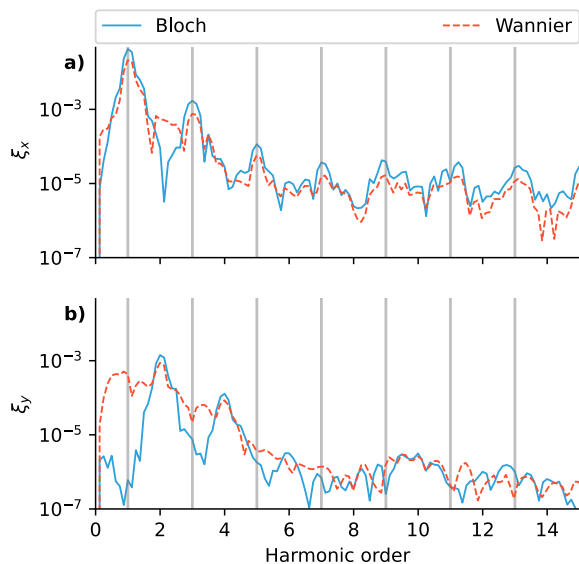


FIG. 6. HHG spectra of the h-BN system along the  $x$  and  $y$  axis derived from the current calculated directly from the Bloch states or from the Wannier centers (Eq. (13))

tem itself is a 2D lattice, and we only present the non-trivial results that are observed along the lattice plane, the calculations are performed in the full 3D real-space grid. The simulation is done with Hartwigsen-Goedecker-Hutter (HGH) pseudo-potentials[66] and corresponding local density approximation (LDA) exchange-correlation functionals, and lattice dimension of  $a = 4.76(a_0)$ . For the laser driving we take only  $n_{\text{cyc}} = 8$  and focus on the results with a peak laser intensity of  $I = 10^{11}(\text{W}/\text{cm}^2)$  and wavelength of  $\lambda = 800(\text{nm})$ . The simulation was done in a real-space grid with spacing  $\Delta a = 0.38(a_0)$ , a  $k$ -space grid of  $27 \times 27 \times 1$ , and a time step of  $\Delta t = 0.29(\hbar/E_h)$ . In this simulation we only sample the time-dependent Wannier functions every 20 time steps.

The HHG spectra of this system has previously been investigated using first-principles methods and model calculations alike[36, 67, 68].

Looking at the HHG spectra of this system in Fig. 6 we find a weaker but still relatively good agreement between the Wannier function derived spectra and the reference one along the driving axis  $x$ . The fact that the agreement is not as good as in the previous model case is to be expected as we are performing various conceptual leaps, in that we are now applying TD-DFT functionals approximations, we are using a coarser time, space and  $k$ -space grid, we are evaluating a shorter laser driving, and we are evaluating the time-dependent Wannier functions less frequently. It is natural that more numerical errors accumulate, and in light of those factors, the fact that the HHG spectra still agree that much, however, is promising.

We next consider the HHG spectra along the  $y$ -axis, where we see a stronger disagreement. To understand

the cause of this deviation, we look at the raw time-dependent currents which we show in Fig. 7 along with the driving laser profile. Here we do not apply the Gaussian filtering, and we scale the laser driving, the reference current and the total Wannier current to their highest absolute value for plotting visibility. Here we want to point out how each Wannier function contribute to the total Wannier current. Along both the  $x$  and  $y$  axis we have significant cancellation of currents as we have similarly seen in the non-interacting model in Fig. 5, but in this case, the cancelling oscillations exceed the total current, especially along the  $y$ -axis where the difference is more than one order of magnitude. This, combined this with how the reference HHG spectra along the  $y$ -axis is two orders of magnitude smaller, and the limitations of the simulations that we previously mentioned, it is acceptable to find such deviations, due to the numerical limitations.

We should also disregard completely the theoretical limitations of the time-dependent Wannier functions defined from Eqs. (1) and (4). Throughout this analysis, we have evaluated the Wannier current by considering the Wannier function of a single unit cell, effectively disregarding the contribution of the dynamics in the many-body representation. In Appendix B we evaluate the propagator of the non-interacting system to find one source of deviation due to resonant excitation. We expect that with further refinement of the time-dependent Wannier function definition and more converged simulation parameters, we would find a more optimal single-particle basis set to represent the dynamics of the many-body interacting system.

#### IV. CONCLUSION

The main result of this work is the definition of the time-dependent Wannier functions that can be efficiently performed on top of well-established first-principles calculation methods, primarily the real-time TD-DFT. In comparison with other proposed definitions for the time-dependent Wannier functions, the method developed here avoids the most expensive part of maximally localizing the basis set. The dynamical polarization model is shown to give good agreements of the current density calculations if we compensate for the dephasing factor of the Wannier states.

While other time-dependent lattice basis, such as the Peierls basis set, require an extensive basis including the initial unoccupied bands and various lattice sites[35, 64, 69], with the time-dependent Wannier functions we are able to limit the necessary basis set to a few of the occupied bands and a single lattice site. This results in a much simpler lattice model that can also be used to study strongly correlated materials, besides the applications we demonstrate here.

While we here have only explored the applicability of the time-dependent Wannier functions for extract-

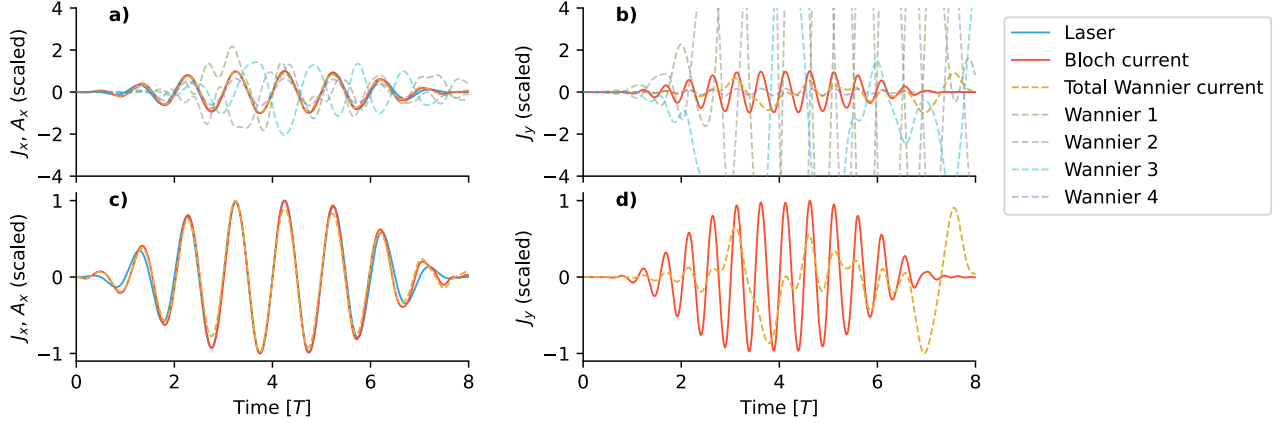


FIG. 7. Applied laser and currents of the h-BN system calculated directly from the Bloch states or from the Wannier centers (Eq. (13)).

ing some physical intuition of the underlying dynamics and as a tool for analyzing non-linear electronic dynamics, there is a vast range of further applications to explore, from improving the TD-DFT calculations, to visualizing and more efficiently calculating the dynamic observables. Looking forward, we believe that time-dependent Wannier functions will prove useful in the evolving field of ultrafast dynamics in solids, especially moving towards strongly correlated materials[60, 70–73], phonon dynamics[55, 63, 74, 75], excitonic effects[76–82], superconductivity[83, 84], etc. These time-dependent basis can prove useful in state of the art calculation methods for highly correlated systems[85, 86].

## V. ACKNOWLEDGEMENTS

This work was supported by the Cluster of Excellence “CUI:Advanced Imaging of Matter” of the Deutsche Forschungsgemeinschaft (DFG) (EXC 2056 and SFB925), and the Max Planck-New York City Center for Non-Equilibrium Quantum Phenomena. The Flatiron Institute is a division of the Simons Foundation.

### Appendix A: Relation to other basis sets

In order to examine the relation of the time-dependent Wannier functions with other commonly used basis like the Peierls basis or the Houston basis, we look at the time-dependent non-interacting electron system, for which we can express the time-dependent Schrödinger

equation as

$$\psi_{n\mathbf{k}}^{\mathbf{A}}(\mathbf{r}, t) = \langle \mathbf{r} | \psi_{n\mathbf{k}}^{\mathbf{A}}(t) \rangle = e^{-i\frac{1}{\hbar}E_{n\mathbf{k}}^0 t} e^{i(\mathbf{k} + \frac{e}{\hbar}\mathbf{A}(t))\mathbf{r}} u_{n\mathbf{k}}(\mathbf{r}), \quad (\text{A1})$$

$$C_{n\mathbf{k}}^i(t) = \langle \psi_{n\mathbf{k}}^{\mathbf{A}}(t) | \Psi_{i\mathbf{k}}(t) \rangle, \quad (\text{A2})$$

$$\partial_t C_{n\mathbf{k}}^i(t) = -e \frac{\partial \mathbf{A}(t)}{\partial t} \sum_m \mathbf{D}_{nm}^{\mathbf{k}}(t) C_{m\mathbf{k}}^i(t), \quad (\text{A3})$$

where  $\psi$  is an auxiliary basis set which we use here for decomposing the dynamics of the propagator,  $C_{n\mathbf{k}}^i$  is the time-dependent projection of the Bloch wave function  $\Psi_{i\mathbf{k}}$  on the time-dependent wave function  $\psi_{n\mathbf{k}}$ , and  $\mathbf{D}_{nm}^{\mathbf{k}}(t)$  is constructed from the transition dipole moment  $\mathbf{D}_{nm}^{\mathbf{k}}$

$$\mathbf{D}_{nm}^{\mathbf{k}}(t) = e^{-i\frac{1}{\hbar}(E_{m\mathbf{k}}^0 - E_{n\mathbf{k}}^0)t} \mathbf{D}_{nm}^{\mathbf{k}}, \quad (\text{A4})$$

$$\mathbf{D}_{nm}^{\mathbf{k}} = \int d\mathbf{r} u_{n\mathbf{k}}^*(\mathbf{r}) \mathbf{r} u_{m\mathbf{k}}(\mathbf{r}). \quad (\text{A5})$$

More details on this derivation are provided in Appendix B. In this derivation we are assuming the dipole approximation. Here we point out that the outside the resonance regime, Eq. (A4) oscillates rapidly such that Eq. (A3) approximates to a constant, and we can take Eq. (A1) to approximate the time-dependent Bloch states.

We apply the basis Eq. (A1) to Eq. (1)

$$\Phi_{n\mathbf{R}}(\mathbf{r}, t) \approx \sum_i \int_{BZ} U_{i\mathbf{k}}^{n\mathbf{R}} f_{i\mathbf{k}}(t) \psi_{i\mathbf{k}}^{\mathbf{A}}(\mathbf{r}, t) d^3\mathbf{k}, \quad (\text{A6})$$

$$\approx P^{\mathbf{AC}}(\mathbf{r}, t) \sum_i \int_{BZ} P_{i\mathbf{k}}^{n\mathbf{D}}(t) U_{i\mathbf{k}}^{n\mathbf{R}} \Psi'_{i\mathbf{k}}(\mathbf{r}, t) d^3\mathbf{k}, \quad (\text{A7})$$

where we group the time-dependent effects into a phase acceleration  $P^{\mathbf{AC}}$ , common for all Wannier functions and dependent only on the laser profile, the main dephasing

contribution  $P^D$  that we investigated in Section II, and the remaining Bloch state dynamics  $\Psi'$  that are covered in Eq. (A3)

$$P^{AC}(\mathbf{r}, t) = e^{i\frac{e}{\hbar}\mathbf{A}(t)\mathbf{r}}, \quad (\text{A8})$$

$$P_{i\mathbf{k}}^{nD}(t) \approx e^{-i\frac{1}{\hbar}E_{n\mathbf{k}}^0 t} f_{i\mathbf{k}}(t), \quad (\text{A9})$$

$$\Psi'_{i\mathbf{k}}(\mathbf{r}, t) \approx \sum_j C_{i\mathbf{k}}^j(t) e^{i\mathbf{k}\mathbf{r}} u_{j\mathbf{k}}(\mathbf{r}), \quad (\text{A10})$$

$$(\text{A11})$$

$P^{AC}$  does not contribute to the dynamics of Wannier centers or Wannier spread,  $P^D$  is close to unity in the Wannier functions  $f^{\text{int}}$ , and the only remaining effects come from the excitation dynamics in Eq. (A3) through  $\Psi'$ . The dynamics in  $\Psi'$  are the main dynamics that we see in Sections II and III.

Comparing this expression with Peierls basis  $\Phi^P$  and the Houston basis  $\Psi^H$

$$\Phi_{n\mathbf{R}}^P(\mathbf{r}, t) = e^{i\frac{e}{\hbar}\mathbf{A}(t)\mathbf{r}} \Phi_{n\mathbf{R}}(\mathbf{r}, 0), \quad (\text{A12})$$

$$\Psi_{i\mathbf{k}}^H(\mathbf{r}, t) = e^{i\frac{e}{\hbar}\mathbf{A}(t)\mathbf{r}} \Psi_{i\mathbf{k}+\mathbf{A}}(\mathbf{r}, 0), \quad (\text{A13})$$

we can see how all of these basis sets merely account for the  $P^{AC}$  contribution, while the remaining dynamics have to be included by expanding the basis set into the unoccupied states and/or the many-body coefficients. When we consider that the Peierls substitution is often performed on a single band basis for computational efficiency, we can see how the dynamics in Eq. (A3) can be completely overlooked.

## Appendix B: Non-interacting propagator

In Appendix A we have referenced the exact propagator of non-interacting systems, and in this appendix we will elaborate on how we have derived it for the sake

of completeness. We start from the time-independent Hamiltonian

$$\hat{H}^0 = \frac{1}{2m} \hat{\mathbf{p}}^2 + \hat{V}, \quad (\text{B1})$$

where  $\mathbf{p}$  and  $V$  are the momentum and spatially periodic potential, respectively. Let's consider we have solved the time-independent Schrödinger equation to get the eigenstates and eigenvalues

$$\hat{H}^0 |\Psi_{i\mathbf{k}}^0\rangle = E_{i\mathbf{k}}^0 |\Psi_{i\mathbf{k}}^0\rangle, \quad (\text{B2})$$

$$\Psi_{i\mathbf{k}}^0(\mathbf{r}) = \langle \mathbf{r} | \Psi_{i\mathbf{k}}^0 \rangle = e^{i\mathbf{k}\mathbf{r}} u_{i\mathbf{k}}(\mathbf{r}). \quad (\text{B3})$$

For the laser interaction, we take the velocity gauge Hamiltonian

$$\hat{H}(t) = \frac{1}{2m} (\hat{\mathbf{p}} - e\mathbf{A}(t))^2 + \hat{V}, \quad (\text{B4})$$

where  $e$  is the charge of the electron and  $\mathbf{A}$  is the applied laser field. For simplicity, we are taking the dipole approximation, ignoring the spatial variation of  $\mathbf{A}$ . We solve the time-dependent Schrödinger equation using the basis defined in Eq. (A1). This basis is an instantaneous eigenbasis of the time-dependent Hamiltonian

$$\langle \psi_{m\mathbf{k}'}^{\mathbf{A}}(t) | \hat{H}(t) | \psi_{n\mathbf{k}}^{\mathbf{A}}(t) \rangle = \delta_{mn} \delta(\mathbf{k}' - \mathbf{k}) E_{n\mathbf{k}}^0. \quad (\text{B5})$$

We solve the time-dependent Schrödinger equation using the overlap

$$C_{n\mathbf{k}'}^{i\mathbf{k}}(t) = \langle \psi_{n\mathbf{k}'}^{\mathbf{A}}(t) | \Psi_{i\mathbf{k}}(t) \rangle, \quad (\text{B6})$$

where  $\Psi_{i\mathbf{k}}(t)$  is the time-dependent wave function of the non-interacting electron with the initial condition

$$|\Psi_{i\mathbf{k}}(0)\rangle = |\Psi_{i\mathbf{k}}^0\rangle. \quad (\text{B7})$$

Expanding the time-dependent Schrödinger equation on this basis we get

$$\langle \psi_{n\mathbf{k}'}^{\mathbf{A}}(t) | i\hbar \partial_t | \Psi_{i\mathbf{k}}(t) \rangle = \langle \psi_{n\mathbf{k}'}^{\mathbf{A}}(t) | \hat{H}(t) | \Psi_{i\mathbf{k}}(t) \rangle, \quad (\text{B8})$$

$$\sum_m \int d\mathbf{k}'' \langle \psi_{n\mathbf{k}'}^{\mathbf{A}}(t) | i\hbar \partial_t | \psi_{m\mathbf{k}''}^{\mathbf{A}}(t) \rangle \langle \psi_{m\mathbf{k}''}^{\mathbf{A}}(t) | \Psi_{i\mathbf{k}}(t) \rangle = E_{n\mathbf{k}'}^0 C_{n\mathbf{k}'}^{i\mathbf{k}}(t), \quad (\text{B9})$$

$$\sum_m \int d\mathbf{k}'' \left[ -e \frac{\partial \mathbf{A}(t)}{\partial t} \int d\mathbf{r} \langle \psi_{n\mathbf{k}'}^{\mathbf{A}}(t) | \hat{\mathbf{r}} | \psi_{m\mathbf{k}''}^{\mathbf{A}}(t) \rangle + \delta_{mn} \delta(\mathbf{k}' - \mathbf{k}'') (i\hbar \partial_t + E_{m\mathbf{k}''}^0) \right] C_{m\mathbf{k}''}^{i\mathbf{k}}(t) = E_{n\mathbf{k}'}^0 C_{n\mathbf{k}'}^{i\mathbf{k}}(t). \quad (\text{B10})$$

We denote  $\mathbf{D}_{nm}^{\mathbf{k}'\mathbf{k}''}(t)$  constructed from the transition

dipole moment  $\mathbf{D}_{nm}^{\mathbf{k}'\mathbf{k}''}$  as

$$\mathbf{D}_{nm}^{\mathbf{k}'\mathbf{k}''}(t) = \langle \psi_{n\mathbf{k}'}^{\mathbf{A}}(t) | \hat{\mathbf{r}} | \psi_{m\mathbf{k}''}^{\mathbf{A}}(t) \rangle, \quad (\text{B11})$$

$$= e^{-i\frac{1}{\hbar}(E_{m\mathbf{k}''}^0 - E_{n\mathbf{k}'}^0)t} \mathbf{D}_{nm}^{\mathbf{k}'\mathbf{k}''}, \quad (\text{B12})$$

$$\mathbf{D}_{nm}^{\mathbf{k}'\mathbf{k}''} = \delta(\mathbf{k}' - \mathbf{k}'') \int d\mathbf{r} u_{n\mathbf{k}}^*(\mathbf{r}) \mathbf{r} u_{m\mathbf{k}}(\mathbf{r}). \quad (\text{B13})$$



Substituting this into Eq. (B10) and simplifying the dirac deltas we get

$$\partial_t C_{nk'}^{ik}(t) = -e \frac{\partial \mathbf{A}(t)}{\partial t} \sum_m \mathbf{D}_{nm}^{\mathbf{k}'}(t) C_{mk'}^{ik}(t), \quad (\text{B14})$$

or considering the initial condition

$$C_{nk'}^{ik}(0) = \delta_{in} \delta(\mathbf{k} - \mathbf{k}'), \quad (\text{B15})$$

we can simplify the equation of motion by ignoring  $\mathbf{k}' \neq \mathbf{k}$  and we get the form in Eq. (A3).

- 
- [1] G. H. Wannier, The structure of electronic excitation levels in insulating crystals, *Physical Review* **52**, 191–197 (1937).
- [2] N. Marzari, A. A. Mostofi, J. R. Yates, I. Souza, and D. Vanderbilt, Maximally localized Wannier functions: Theory and applications, *Reviews of Modern Physics* **84**, 1419 (2012).
- [3] H. Abu-Farsakh and A. Qteish, Ionicity scale based on the centers of maximally localized wannier functions, *Physical Review B* **75**, 085201 (2007).
- [4] R. Evarestov, V. Smirnov, and D. Usvyat, Local properties of the electronic structure of cubic srtio3, batio3 and pbtio3 crystals, analysed using wannier-type atomic functions, *Solid State Communications* **127**, 423–426 (2003).
- [5] G. Cangiani, A. Baldereschi, M. Posternak, and H. Krakauer, Born charge differences of tio2 polytypes: Multipole expansion of wannier charge densities, *Physical Review B* **69**, 121101(R) (2004).
- [6] R. D. King-Smith and D. Vanderbilt, Theory of polarization of crystalline solids, *Physical Review B* **47**, 1651 (1993).
- [7] R. Resta, Modern theory of polarization in ferroelectrics, *Ferroelectrics* **151**, 49–58 (1994).
- [8] R. Resta and D. Vanderbilt, Theory of polarization: A modern approach, in *Physics of Ferroelectrics* (Springer Berlin Heidelberg, 2007) p. 31–68.
- [9] D. Vanderbilt and R. Resta, Chapter 5 quantum electrostatics of insulators: Polarization, wannier functions, and electric fields, in *Conceptual Foundations of Materials - A Standard Model for Ground- and Excited-State Properties* (Elsevier, 2006) p. 139–163.
- [10] P. Sony and A. Shukla, Ab initio wannier-function-based correlated calculations of born effective charges of crystalline li2O and licl, *Physical Review B* **77**, 075130 (2008).
- [11] S. S. Tsirkin, High performance wannier interpolation of berry curvature and related quantities with wannierberri code, *npj Computational Materials* **7**, 10.1038/s41524-021-00498-5 (2021).
- [12] J.-M. Lihm and C.-H. Park, Wannier function perturbation theory: Localized representation and interpolation of wave function perturbation, *Phys. Rev. X* **11**, 041053 (2021).
- [13] M. Nakagawa, R.-J. Slager, S. Higashikawa, and T. Oka, Wannier representation of floquet topological states, *Phys. Rev. B* **101**, 075108 (2020).
- [14] I. Souza, J. Ñiguez, and D. Vanderbilt, Dynamics of Berry-phase polarization in time-dependent electric fields, *Physical Review B* **69**, 085106 (2004).
- [15] D. C. Yost, Y. Yao, and Y. Kanai, Propagation of maximally localized Wannier functions in real-time TDDFT, *The Journal of Chemical Physics* **150**, 194113 (2019).
- [16] F. Giustino, M. L. Cohen, and S. G. Louie, Electron-phonon interaction using wannier functions, *Physical Review B* **76**, 165108 (2007).
- [17] J. Noffsinger, F. Giustino, B. D. Malone, C.-H. Park, S. G. Louie, and M. L. Cohen, Epw: A program for calculating the electron–phonon coupling using maximally localized wannier functions, *Computer Physics Communications* **181**, 2140–2148 (2010).
- [18] S. Poncé, E. Margine, C. Verdi, and F. Giustino, Epw: Electron–phonon coupling, transport and superconducting properties using maximally localized wannier functions, *Computer Physics Communications* **209**, 116–133 (2016).
- [19] J.-J. Zhou, J. Park, I.-T. Lu, I. Maliyov, X. Tong, and M. Bernardi, Perturbo: A software package for ab initio electron–phonon interactions, charge transport and ultrafast dynamics, *Computer Physics Communications* **264**, 107970 (2021).
- [20] W. Ku, H. Rosner, W. E. Pickett, and R. T. Scalettar, Insulating ferromagnetism in la4ba2cu2o10: An ab initio wannier function analysis, *Physical Review Letters* **89**, 167204 (2002).
- [21] F. Aryasetiawan, T. Miyake, and R. Sakuma, The LDA+DMFT approach to strongly correlated materials (Forschungszentrum Jülich, 2011) Chap. The Constrained RPA Method for Calculating the Hubbard U from First-Principles.
- [22] R. Zhou, D. C. Yost, and Y. Kanai, First-principles demonstration of nonadiabatic thoulless pumping of electrons in a molecular system, *The Journal of Physical Chemistry Letters* **12**, 4496–4503 (2021).
- [23] S. Ghimire and D. A. Reis, High-harmonic generation from solids, *Nature Physics* **15**, 10–16 (2018).
- [24] S. Ghimire, G. Ndabashimiye, A. D. DiChiara, E. Sistrunk, M. I. Stockman, P. Agostini, L. F. DiMauro, and D. A. Reis, Strong-field and attosecond physics in solids, *Journal of Physics B: Atomic, Molecular and Optical Physics* **47**, 204030 (2014).
- [25] L. Yue and M. B. Gaarde, Introduction to theory of high-harmonic generation in solids: tutorial, *Journal of the Optical Society of America B* **39**, 535 (2022).
- [26] M. S. Mrudul and G. Dixit, High-harmonic generation from monolayer and bilayer graphene, *Physical Review B* **103**, 094308 (2021).
- [27] N. Rana and G. Dixit, Probing phonon-driven symmetry alterations in graphene via high-order-harmonic spectroscopy, *Physical Review A* **106**, 053116 (2022).
- [28] D. Bauer and K. K. Hansen, High-harmonic generation in

- solids with and without topological edge states, *Physical Review Letters* **120**, 177401 (2018).
- [29] H. Jürß and D. Bauer, High-harmonic generation in suschrieffler-heeger chains, *Physical Review B* **99**, 195428 (2019).
- [30] R. E. F. Silva, A. Jiménez-Galán, B. Amorim, O. Smirnova, and M. Ivanov, Topological strong-field physics on sub-laser-cycle timescale, *Nature Photonics* **13**, 849–854 (2019).
- [31] D. Baykusheva, A. Chacón, D. Kim, D. E. Kim, D. A. Reis, and S. Ghimire, Strong-field physics in three-dimensional topological insulators, *Physical Review A* **103**, 023101 (2021).
- [32] A. Chacón, D. Kim, W. Zhu, S. P. Kelly, A. Dauphin, E. Pisanty, A. S. Maxwell, A. Picón, M. F. Ciappina, D. E. Kim, C. Ticknor, A. Saxena, and M. Lewenstein, Circular dichroism in higher-order harmonic generation: Heraldng topological phases and transitions in chern insulators, *Physical Review B* **102**, 134115 (2020).
- [33] Y.-Y. Lv, J. Xu, S. Han, C. Zhang, Y. Han, J. Zhou, S.-H. Yao, X.-P. Liu, M.-H. Lu, H. Weng, Z. Xie, Y. B. Chen, J. Hu, Y.-F. Chen, and S. Zhu, High-harmonic generation in weyl semimetal  $\beta - \text{wp}_2$  crystals, *Nature Communications* **12**, 10.1038/s41467-021-26766-y (2021).
- [34] T. T. Luu and H. J. Wörner, Measurement of the berry curvature of solids using high-harmonic spectroscopy, *Nature Communications* **9**, 10.1038/s41467-018-03397-4 (2018).
- [35] T. Ikemachi, Y. Shinohara, T. Sato, J. Yumoto, M. Kuwata-Gonokami, and K. L. Ishikawa, Trajectory analysis of high-order-harmonic generation from periodic crystals, *Physical Review A* **95**, 043416 (2017).
- [36] R. E. F. Silva, F. Martín, and M. Ivanov, High harmonic generation in crystals using maximally localized wannier functions, *Physical Review B* **100**, 195201 (2019).
- [37] G. G. Brown, A. Jiménez-Galán, R. E. F. Silva, and M. Ivanov, Ultrafast dephasing in solid-state high harmonic generation: macroscopic origin revealed by real-space dynamics [invited], *Journal of the Optical Society of America B* **41**, B40 (2024).
- [38] E. N. Osika, A. Chacón, L. Ortmann, N. Suárez, J. A. Pérez-Hernández, B. Szafran, M. F. Ciappina, F. Sols, A. S. Landsman, and M. Lewenstein, Wannier-bloch approach to localization in high-harmonics generation in solids, *Physical Review X* **7**, 021017 (2017).
- [39] F. Catoire, H. Bachau, Z. Wang, C. Blaga, P. Agostini, and L. F. DiMauro, Wannier representation of intraband high-order harmonic generation, *Physical Review Letters* **121**, 143902 (2018).
- [40] A. M. Parks, G. Ernotte, A. Thorpe, C. R. McDonald, P. B. Corkum, M. Taucer, and T. Brabec, Wannier quasi-classical approach to high harmonic generation in semiconductors, *Optica* **7**, 1764 (2020).
- [41] Y. Murakami, M. Eckstein, and P. Werner, High-harmonic generation in mott insulators, *Physical Review Letters* **121**, 057405 (2018).
- [42] J. B. Krieger and G. J. Iafrate, Time evolution of bloch electrons in a homogeneous electric field, *Physical Review B* **33**, 5494 (1986).
- [43] S. A. Sato and K. Yabana, Efficient basis expansion for describing linear and nonlinear electron dynamics in crystalline solids, *Physical Review B* **89**, 224305 (2014).
- [44] S. A. Sato, M. Lucchini, M. Volkov, F. Schlaepfer, L. Gallmann, U. Keller, and A. Rubio, Role of intraband transitions in photocarrier generation, *Physical Review B* **98**, 035202 (2018).
- [45] C. W. Byun, M.-H. Lee, and N. N. Choi, High-order harmonic generation from solids using houston states, *Journal of the Korean Physical Society* **78**, 662–670 (2021).
- [46] F. H. M. Faisal and J. Z. Kamiński, Floquet-bloch theory of high-harmonic generation in periodic structures, *Physical Review A* **56**, 748 (1997).
- [47] J.-Z. Jin, H. Liang, X.-R. Xiao, M.-X. Wang, S.-G. Chen, X.-Y. Wu, Q. Gong, and L.-Y. Peng, Contribution of floquet-bloch states to high-order harmonic generation in solids, *Physical Review A* **100**, 013412 (2019).
- [48] M. Wu, S. Ghimire, D. A. Reis, K. J. Schafer, and M. B. Gaarde, High-harmonic generation from bloch electrons in solids, *Physical Review A* **91**, 043839 (2015).
- [49] T. N. Ikeda, K. Chinzei, and H. Tsunetsugu, Floquet-theoretical formulation and analysis of high-order harmonic generation in solids, *Physical Review A* **98**, 063426 (2018).
- [50] A. Galler, A. Rubio, and O. Neufeld, Mapping light-dressed floquet bands by highly nonlinear optical excitations and valley polarization, *The Journal of Physical Chemistry Letters* **14**, 11298–11304 (2023).
- [51] O. Neufeld, W. Mao, H. Hübener, N. Tancogne-Dejean, S. A. Sato, U. De Giovannini, and A. Rubio, Time- and angle-resolved photoelectron spectroscopy of strong-field light-dressed solids: Prevalence of the adiabatic band picture, *Physical Review Research* **4**, 033101 (2022).
- [52] D. Dimitrovski, T. G. Pedersen, and L. B. Madsen, Floquet-bloch shifts in two-band semiconductors interacting with light, *Physical Review A* **95**, 063420 (2017).
- [53] M. A.L. Marques, N. T. Maitra, F. M.S. Nogueira, G. E.K.U., and A. Rubio, eds., *Fundamentals of Time-Dependent Density Functional Theory* (Springer Berlin Heidelberg, 2012).
- [54] O. Neufeld, N. Tancogne-Dejean, H. Hübener, U. De Giovannini, and A. Rubio, Are there universal signatures of topological phases in high-harmonic generation? probably not., *Physical Review X* **13**, 031011 (2023).
- [55] O. Neufeld, J. Zhang, U. De Giovannini, H. Hübener, and A. Rubio, Probing phonon dynamics with multidimensional high harmonic carrier-envelope-phase spectroscopy, *Proceedings of the National Academy of Sciences* **119**, 10.1073/pnas.2204219119 (2022).
- [56] J. Zhang, O. Neufeld, N. Tancogne-Dejean, I.-T. Lu, H. Hübener, U. De Giovannini, and A. Rubio, Enhanced high harmonic efficiency through phonon-assisted photodoping effect, *npj Computational Materials* **10**, 10.1038/s41524-024-01399-z (2024).
- [57] O. Neufeld, N. Tancogne-Dejean, U. De Giovannini, H. Hübener, and A. Rubio, Attosecond magnetization dynamics in non-magnetic materials driven by intense femtosecond lasers, *npj Computational Materials* **9**, 10.1038/s41524-023-00997-7 (2023).
- [58] N. Tancogne-Dejean, F. G. Eich, and A. Rubio, Effect of spin-orbit coupling on the high harmonics from the topological dirac semimetal  $\text{na}_3\text{Bi}$ , *npj Computational Materials* **8**, 10.1038/s41524-022-00831-6 (2022).
- [59] N. Tancogne-Dejean, O. D. Mücke, F. X. Kärtner, and A. Rubio, Impact of the electronic band structure in high-harmonic generation spectra of solids, *Physical Review Letters* **118**, 087403 (2017).
- [60] N. Tancogne-Dejean, M. A. Sentef, and A. Rubio, Ultrafast modification of hubbard  $u$  in a strongly corre-

- lated material: Ab initio high-harmonic generation in nio, *Physical Review Letters* **121**, 097402 (2018).
- [61] O. Neufeld and O. Cohen, Background-free measurement of ring currents by symmetry-breaking high-harmonic spectroscopy, *Physical Review Letters* **123**, 103202 (2019).
- [62] N. Tancogne-Dejean, M. J. T. Oliveira, X. Andrade, H. Appel, C. H. Borca, G. Le Breton, F. Buchholz, A. Castro, S. Corni, A. A. Correa, U. De Giovannini, A. Delgado, F. G. Eich, J. Flick, G. Gil, A. Gomez, N. Helbig, H. Hübener, R. Jestädt, J. Jornet-Somoza, A. H. Larsen, I. V. Lebedeva, M. Lüders, M. A. L. Marques, S. T. Ohlmann, S. Pipolo, M. Rampp, C. A. Rozzi, D. A. Strubbe, S. A. Sato, C. Schäfer, I. Theophilou, A. Welden, and A. Rubio, Octopus, a computational framework for exploring light-driven phenomena and quantum dynamics in extended and finite systems, *The Journal of Chemical Physics* **152**, 10.1063/1.5142502 (2020).
- [63] J. Zhang, Z. Wang, F. Lengers, D. Wigger, D. E. Reiter, T. Kuhn, H. J. Wörner, and T. T. Luu, High-harmonic spectroscopy probes lattice dynamics, *Nature Photonics* **18**, 792–798 (2024).
- [64] X. Liu, X. Zhu, X. Zhang, D. Wang, P. Lan, and P. Lu, Wavelength scaling of the cutoff energy in the solid high harmonic generation, *Optics Express* **25**, 29216 (2017).
- [65] O. Neufeld, D. Podolsky, and O. Cohen, Floquet group theory and its application to selection rules in harmonic generation, *Nature Communications* **10**, 10.1038/s41467-018-07935-y (2019).
- [66] C. Hartwigsen, S. Goedecker, and J. Hutter, Relativistic separable dual-space gaussian pseudopotentials from h to rn, *Physical Review B* **58**, 3641 (1998).
- [67] G. Le Breton, A. Rubio, and N. Tancogne-Dejean, High-harmonic generation from few-layer hexagonal boron nitride: Evolution from monolayer to bulk response, *Physical Review B* **98**, 165308 (2018).
- [68] D. Kim, Y. Lee, A. Chacón, and D.-E. Kim, Effect of interlayer coupling and symmetry on high-order harmonic generation from monolayer and bilayer hexagonal boron nitride, *Symmetry* **14**, 84 (2022).
- [69] A. Thorpe, N. Boroumand, A. M. Parks, E. Goulielmakis, and T. Brabec, High harmonic generation in solids: Real versus virtual transition channels, *Physical Review B* **107**, 075135 (2023).
- [70] R. E. F. Silva, I. V. Blinov, A. N. Rubtsov, O. Smirnova, and M. Ivanov, High-harmonic spectroscopy of ultrafast many-body dynamics in strongly correlated systems, *Nature Photonics* **12**, 266–270 (2018).
- [71] V. N. Valmispild, E. Gorelov, M. Eckstein, A. I. Lichtenstein, H. Aoki, M. I. Katsnelson, M. Y. Ivanov, and O. Smirnova, Sub-cycle multidimensional spectroscopy of strongly correlated materials, *Nature Photonics* **18**, 432–439 (2024).
- [72] K. Uchida, G. Mattoni, S. Yonezawa, F. Nakamura, Y. Maeno, and K. Tanaka, High-order harmonic generation and its unconventional scaling law in the mott-insulating  $\text{ca}_2\text{ruo}_4$ , *Physical Review Letters* **128**, 127401 (2022).
- [73] Y. Murakami, K. Uchida, A. Koga, K. Tanaka, and P. Werner, Anomalous temperature dependence of high-harmonic generation in mott insulators, *Physical Review Letters* **129**, 157401 (2022).
- [74] M. R. Bionta, E. Haddad, A. Leblanc, V. Gruson, P. Lassonde, H. Ibrahim, J. Chaillou, N. Émond, M. R. Otto, A. Jiménez-Galán, R. E. F. Silva, M. Ivanov, B. J. Siwick, M. Chaker, and F. m. c. Légaré, Tracking ultrafast solid-state dynamics using high harmonic spectroscopy, *Physical Review Research* **3**, 023250 (2021).
- [75] K. Lively, S. A. Sato, G. Albareda, A. Rubio, and A. Kelly, Revealing ultrafast phonon mediated intervalley scattering through transient absorption and high harmonic spectroscopies, *Physical Review Research* **6**, 013069 (2024).
- [76] Y. Kobayashi, C. Heide, A. C. Johnson, V. Tiwari, F. Liu, D. A. Reis, T. F. Heinz, and S. Ghimire, Floquet engineering of strongly driven excitons in monolayer tungsten disulfide, *Nature Physics* 10.1038/s41567-022-01849-9 (2023).
- [77] V. Chang Lee, L. Yue, M. B. Gaarde, Y.-h. Chan, and D. Y. Qiu, Many-body enhancement of high-harmonic generation in monolayer mos2, *Nature Communications* **15**, 10.1038/s41467-024-50534-3 (2024).
- [78] S. V. B. Jensen, L. B. Madsen, A. Rubio, and N. Tancogne-Dejean, High-harmonic spectroscopy of strongly bound excitons in solids, *Physical Review A* **109**, 063104 (2024).
- [79] E. B. Molinero, B. Amorim, M. Malakhov, G. Cistaro, A. Jiménez-Galán, A. Picón, P. San-José, M. Ivanov, and R. E. F. Silva, Subcycle dynamics of excitons under strong laser fields, *Science Advances* **10**, 10.1126/sciadv.adn6985 (2024).
- [80] M. Udono, K. Sugimoto, T. Kaneko, and Y. Ohta, Excitonic effects on high-harmonic generation in mott insulators, *Physical Review B* **105**, L241108 (2022).
- [81] J. Freudenstein, M. Borsch, M. Meierhofer, D. Afanasiev, C. P. Schmid, F. Sandner, M. Liebich, A. Girnghuber, M. Knorr, M. Kira, and R. Huber, Attosecond clocking of correlations between bloch electrons, *Nature* **610**, 290–295 (2022).
- [82] G. Cohen, J. B. Haber, J. B. Neaton, D. Y. Qiu, and S. Refaely-Abramson, Phonon-driven femtosecond dynamics of excitons in crystalline pentacene from first principles, *Physical Review Letters* **132**, 126902 (2024).
- [83] J. Alcalà, U. Bhattacharya, J. Biegert, M. Ciappina, U. Elu, T. Graß, P. T. Grochowski, M. Lewenstein, A. Palau, T. P. H. Sidiropoulos, T. Steinle, and I. Tyulnev, High-harmonic spectroscopy of quantum phase transitions in a high- $t_c$  superconductor, *Proceedings of the National Academy of Sciences* **119**, 126902 (2022).
- [84] S.-Q. Hu, D.-Q. Chen, L.-L. Du, and S. Meng, Solid-state high harmonic spectroscopy for all-optical band structure probing of high-pressure quantum states, *Proceedings of the National Academy of Sciences* **121**, 10.1073/pnas.2316775121 (2024).
- [85] P. Seth, I. Krivenko, M. Ferrero, and O. Parcollet, Triqs/cthyb: A continuous-time quantum monte carlo hybridisation expansion solver for quantum impurity problems, *Computer Physics Communications* **200**, 274–284 (2016).
- [86] W. T. Tai and M. Claassen, Quantum-geometric light-matter coupling in correlated quantum materials (2023).